Effects of Hydrodynamic Conditions and LiBr Concentration on the Corrosion of Copper in LiBr Absorption Machines

R. Leiva-García, M.J. Muñoz-Portero, J. García-Antón[*], R. Sánchez-Tovar

Ingeniería Electroquímica y Corrosión (IEC), Departamento de Ingeniería Química y Nuclear, E.T.S.I. Industriales,Universidad Politècnica de València E-46071 Valencia, Spain
[*]Universitat Politècnica de València, Spain,
[*]E-mail: jgarciaa@iqn.upv.es

Refrigeration absorption machines are again considered as suitable refrigeration systems and they are replacing compression machines due to the ban of chlorofluorocarbons (CFCs) and the strict regulations of hydrochlorofluorocarbons. Lithium Bromide (LiBr) is one of the most widely used absorbents in refrigeration technology. However, the operating conditions of absorption machines (high concentration and high temperature) can cause serious corrosion problems in the structural materials. Corrosion problems can be enhanced by the hydrodynamic conditions of the system. The present work studies of the influence of hydrodynamic conditions on copper corrosion under different LiBr conditions. Polarisation potentiodynamic curves obtained following ASTM G-5 were used to study the influence of the LiBr concentration and hydrodynamic conditions. Parameters such as corrosion current density and corrosion potential were obtained from the potentiodynamic curves. A rotating disk electrode (RDE) was used to determine the hydrodynamic conditions. Three LiBr solutions of different concentration (400 g/l, 700 g/l, and 850 g/l) at 25 ºC and different rotation rates (0 r.p.m. − 3000 r.p.m.) were used during the tests.Results show that an increase of the bromide concentration and rotation rate favours copper corrosion and enhances anodic dissolution. The effects of the hydrodynamic conditions are smaller at higher LiBr concentrations.

1. INTRODUCTION

The use of chlorofluorocarbons (CFCs) was banned (Montreal Protocol [1], 1987) and their substitutes, i.e. hydrochlorofluorocarbons, are subjected to severe regulations (Kyoto Protocol [2], 1997). Therefore, refrigeration absorption machines are again considered as suitable refrigeration systems. Among the different materials used in the manofacture of absorption machines copper is commonly used in heat exchangers pipes due to copper`s high thermal conductivity. Absorption

machines can use different working fluid such as (NH_3-H_2O) or (H_2O-LiBr). H_2O-LiBr is the most commonly employed refrigerant/absorbent couple in absorption systems due to its favourable thermophysical properties [3, 4]. However, LiBr can cause serious corrosion problems on metallic components in refrigeration systems. Bromides, like chlorides, are aggressive ions and their corrosion effect may be accelerated in absorption machines due to the high temperatures and concentrations reached, particularly in new double-effect systems, which are more efficient. Corrosion of metals in aqueous environments involves at least three steps: (1) electrolyte transport from the bulk solution to the metal surface, (2) electrode exchange at the electrode/solution interface leading to metal loss, and finally, (3) transport of corrosion product from the interface to the bulk solution. Therefore, it is necessary to take into account charge transfer as well as mass transfer. The latter may be modified by the hydrodynamic conditions of the system. Corrosion problems can be enhanced by the hydrodynamic conditions of the fluid [5, 6]. Several works have studied the corrosion of different metals in LiBr solutions under different conditions [7-12].

The present work studies the influence of LiBr concentrations and hydrodynamic conditions on the corrosion of copper. Polarisation potentiodynamic curves at 25 ºC were obtained in three different concentrations (400 g/l, 700 g/l, and 850 g/l) of LiBr solutions and at different rotation rates (0 r.p.m. – 3000 r.p.m.). A rotating disk electrode (RDE) system was employed to produce the different rotation rates. RDE devices are widely used in studies of flow accelerated corrosion under mass transfer control in laminar and turbulent regimes [13-21].

2. EXPERIMENTAL PROCEDURE

2.1. Materials

The working electrodes were made of copper and were cylindrically shaped (55 mm long and 9 mm in diameter) and covered with Teflon. An area of 0.64 cm^2 was exposed to the electrolyte. Prior to the electrochemical tests, the samples were wet abraded from 220 SiC (Silicon Carbide) grit to a 4000 SiC grit finish, and finally rinsed with distilled water. Later, the working electrode was connected to a RDE system to change the hydrodynamic conditions. The employed cell was a glass vertical cell with different inlets and a thermostatic jacket, which maintained the temperature constant at 25 ºC. The potential was measured against an Ag/AgCl with 3M KCl reference electrode. The counter electrode was made of platinum.

2.2. Polarisation potentiodynamic curves

Polarisation potentiodynamic curves were carried out in three aqueous LiBr solutions of different concentrations (400 g/l, 700 g/l, and 850 g/l) prepared from purissimun LiBr of Panreac. Table 1 shows the rotation rates in revolutions per minute (r.p.m.) and the Reynolds number for the different studied LiBr concentrations. In all cases, the tests were repeated at least three times. The Reynolds number (Re), which is shown in Table 1, could be calculated from the angular velocity:

$$\mathrm{Re} = \frac{\omega \cdot r^2}{\upsilon} = \frac{\rho \cdot 2 \cdot \pi \cdot f \cdot r^2}{\mu \cdot 60}$$

(1)

where ω is the angular velocity (rad/s), f is the rotation rate (r.p.m.), r is the electrode radius (cm), υ is the kinematic viscosity (cm^2/s), ρ is the solution density (g/cm^3), and μ is the absolute viscosity (g/s·cm).

Table 1. Reynolds numbers of the copper RDE in the different LiBr solutions at 25 ºC.

f (r.p.m.)	Re		
	400 g/l LiBr υ (cm^2/s) = 1.27x10^{-2}	700 g/l LiBr υ (cm^2/s) = 1.91x10^{-2}	850 g/l LiBr υ (cm^2/s) = 2.91x10^{-2}
0	0	0	0
500	834	552	364
1000	1669	1105	729
1500	2503	1657	1094
2000	3338	2209	1458
2500	4172	2762	1823
3000	5006	3314	2187

The polarisation curves were made in LiBr aqueous solution deaireated by bubbling nitrogen for 30 minutes, prior to immersion. During the test, a nitrogen atmosphere was maintained over the liquid surface. The rotation rate of the RDE was set at the beginning of the electrochemical test. Before each polarisation experiment, the open circuit potential (OCP) was recorded for one hour; the OCP value reported here was the arithmetic mean of the last five minutes recorded values [22]. After the OCP test, the specimen potential was reduced progressively to − 1000 mV$_{Ag/AgCl}$; this potential was maintained constant for 300 s in order to create reproducible initial conditions. Then the working electrode potential was scanned from –1000 mV$_{Ag/AgCl}$ to 1000 mV$_{Ag/AgCl}$, using a scan rate of 0.1667 mV/s, according to ASTM G-5 [22]. The polarisation curves were recorded from the cathodic to the anodic direction. These curves were used to calculate Corrosion potential (E$_{corr}$), and corrosion current density (i$_{corr}$) as well as information about the general electrochemical behaviour of the materials was also obtained. Additionally, polarisation potentiodynamic curves were obtained under static conditions using the patented electro-optical devices P-200002525 and P-200002526 [23-26]. These devices permit obtaining images of the electrode surface and electrochemical data simultaneously. Finally, all the tested specimens were observed by optical microscopy.

3. RESULTS AND DISCUSSION

3.1. Open circuit potential

Figure 1 shows the effect of the rotation rate variation and LiBr concentration on the open circuit potential values. OCP values decrease when the rotation rate and LiBr concentration increase.

Higher LiBr concentrations enhance the presence of aggressive anions and make the corrosive system more active. On the other hand, under rotating conditions, the high relative velocity between the electrode and the fluid can induce stress acting on the electrode surface. Therefore, the decrease of the OCP may be due to the damage or loss of the passive film [27].
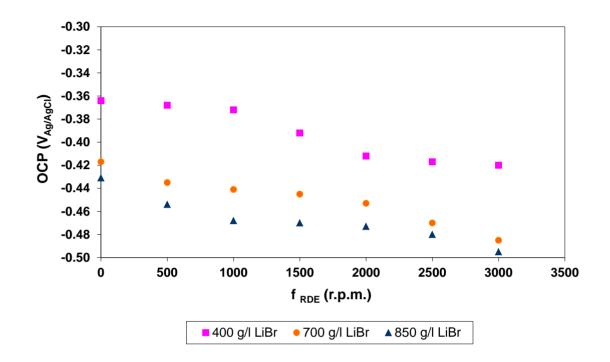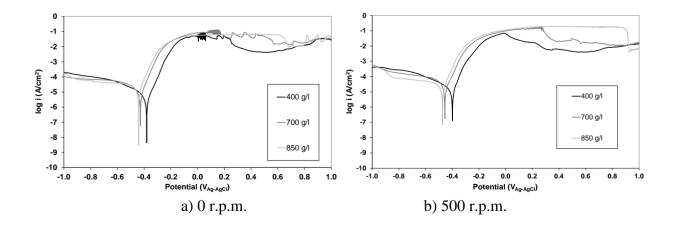

Figure 1. Effect of the rotation rate on the open circuit potential (OCP) of copper in the different aqueous LiBr solutions at 25 ºC.

3.2. *Polarisation potentiodynamic curves*

Figure 2 shows the polarisation curves of copper at the different rotation rates in the 400 g/l, 700 g/l, and 850 g/l LiBr solutions at 25 ºC.
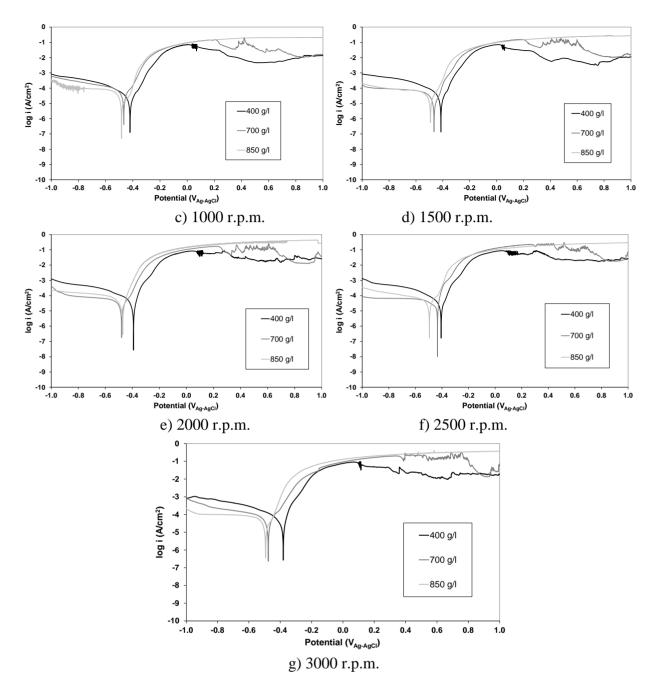

a) 0 r.p.m.   b) 500 r.p.m.

c) 1000 r.p.m.   d) 1500 r.p.m.

e) 2000 r.p.m.   f) 2500 r.p.m.

g) 3000 r.p.m.

Figure 2. Polarisation curves of copper at the different rotation rates in the three used LiBr solutions at 25 ºC.

The current density of the cathodic branch of the potentiodynamic curves is higher for the 400 g/L LiBr solution than for the other solutions.

This tendency can be related to the increase in solution viscosity, which accompanies the increase of LiBr concentration which, subsequently, reduces the cathodic limiting current as shown by the Levich relationship [28].

The current density of the anodic branch is the lowest for the 400 g/l LiBr solution. In the tests carried out in the 400 g/l LiBr solution under static and dynamic conditions and in the 700 g/l LiBr solution under static conditions, an oscillation area appears in the anodic branch. This area corresponds

to a region of rapid formation and dissolution of corrosion products with a certain passivating character [29].

Images of the electrode surface under static conditions taken with the patented electro-optical devices are shown in Figures 3 to 5.
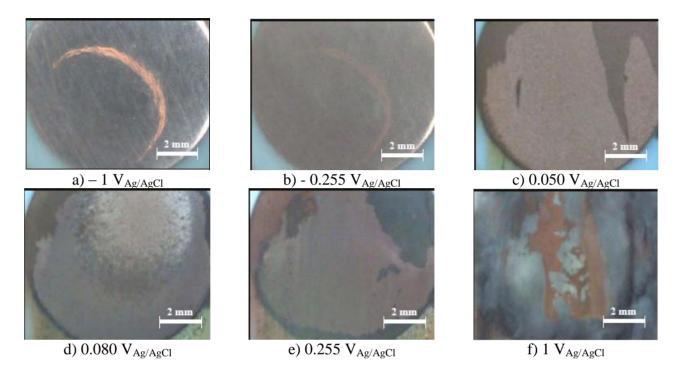

a) -1 $V_{Ag/AgCl}$ b) -0.255 $V_{Ag/AgCl}$ c) 0.050 $V_{Ag/AgCl}$

d) 0.080 $V_{Ag/AgCl}$ e) 0.255 $V_{Ag/AgCl}$ f) 1 $V_{Ag/AgCl}$

Figure 3. Images of the electrode surface obtained at different points of the polarisation curves taken with the electro-optical patented devices in the 400 g/l LiBr solution at 25 ºC under static conditions.

In the case of the 400 g/l LiBr solution, when the potentiodynamic curve begins (Figure 3 a)), the electrode surface is unaffected and presents a metallic shine. When the corrosion potential is reached and current density rises, the anodic dissolution of the electrode begins and the metallic shine of the surface disappears (Figure 3 b)). In the oscillation interval, the corrosion products, which play a certain passivating role, are quickly formed and dissolved on the electrode surface as shown in Figures 3 c) and d). After that, some corrosion products appear on the electrode surface generating anodic peaks in the potentiodynamic curve (Figure 3 e)). Finally, at the end of the potentiodynamic curve, the electrode surface appears completely covered by a blue corrosion product (Figure 3 f)).

In the case of the 700 g/l LiBr solution, the behaviour of the electrode surface is similar. When the anodic branch begins the surface starts dissolving and the metallic shine disappears (Figure 4 b)). After that, the oscillation interval appears and different films of corrosion product form and disappear quickly. On the other hand, when the polarisation curve presents anodic peaks different corrosion products form on the electrode surface (Figure 4 e)). At the end of the tests the surface is completely covered by the corrosion products.
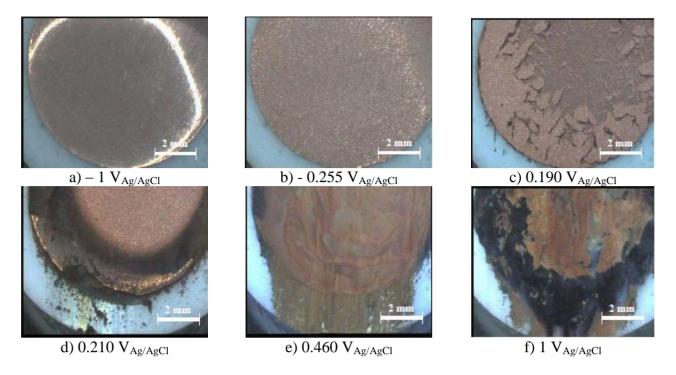
Figure 4. Images of the electrode surface obtained at different points of the polarisation curves taken with the electro-optical patented devices in the 700 g/l LiBr solution at 25 ºC under static conditions.
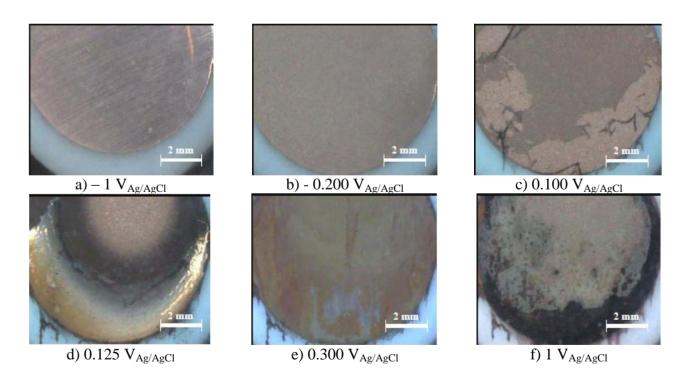

Figure 5. Images of the electrode surface obtained at different points of the polarisation curves taken with the electro-optical patented devices in the 850 g/l LiBr solution at 25 ºC under static conditions.

The evolution of the electrode surface during the polarisation curve of the 850 g/l solution is slightly different than in the other solutions. In this case there is no oscillation interval and the dissolution of the electrode surface happens only once and after that, different corrosion products cover the electrode surface during the dissolution of the copper.

3.3. Corrosion potential

Table 2 shows the corrosion potentials of copper in the three LiBr concentrations at the different rotation rates.

Table 2. Corrosion potential values (E_{corr}) of copper at the different rotation rates in the 400 g/l, 700 g/l, and 850 g/l LiBr solutions at 25 ° C.

	E_{corr} (mV$_{Ag/AgCl}$)		
f (r.p.m.)	400 g/l LiBr	700 g/l LiBr	850 g/l LiBr
0	- 374	- 443	- 443
500	- 397	- 462	- 467
1000	- 400	- 466	- 470
1500	- 407	- 470	- 483
2000	- 410	- 475	- 486
2500	- 415	- 480	- 494
3000	- 420	- 483	- 498

Corrosion potential shifts to more negative values with the rotation rate and LiBr concentration. This trend is similar that observed in the OCP evolution, although E_{corr} values are more negative than OCP ones due to the applied polarisation [30, 31].

Figure 6 represents the E_{corr} in function of ln ω (rad/s). Power, Richie, and Brossard [32, 33] proposed that studying the corrosion potential variation with the rotation rate it is possible to distinguish different corrosion mechanisms:

1)   When the $\Delta(E_{corr})/\Delta$ (ln ω (rad/s)) is positive, the cathodic reaction is controlled by diffusion and the anodic reaction is electrochemically controlled (case 1).

2)   When the $\Delta(E_{corr})/\Delta$ (ln ω (rad/s)) is zero, two cases can be possible: the anodic and cathodic reactions are controlled by diffusion (case 2). Otherwise, the reactions are under electrochemical control (case 3).

3)   When the $\Delta(E_{corr})/\Delta$ (ln ω (rad/s)) is negative, the cathodic reaction is electrochemically controlled and the anodic reaction is controlled by diffusion (case 4).

For the three studied LiBr solutions the $\Delta(E_{corr})/\Delta$ (ln ω) value obtained was negative: - 21.54 mV in the case of the 400 g/l LiBr solution, - 19.3 mV for the 700 g/l solution, and – 18.0 mV for the 850 g/l LiBr solution. Therefore, it corresponds to case 4 when the anodic reaction is controlled by diffusion (under mass transport control) and the cathodic reaction is electrochemically controlled (under activation control).
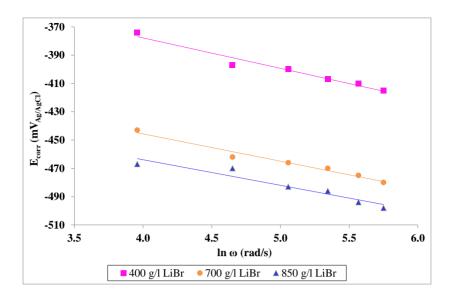
Figure 6. Corrosion potential (E_{corr}) of copper in function of the ln ω (rad/s) in the different aqueous LiBr solutions at 25 ºC.
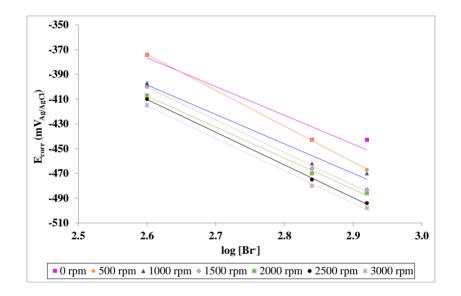

Figure 7. Evolution of the corrosion potential of copper with the logarithm of the LiBr concentration for every rotation rate value at 25 ºC.

In solutions with complexing agents, such as bromide, the anodic dissolution of copper is controlled by the formation of soluble copper species in the Cu(II) state. Then, anodic dissolution of copper is given by the following reaction [33-36]:

$$Cu + 2 \ Br^- \rightarrow (CuBr_2)_S^- + 1 \ e^- \qquad (2)$$

After that, the $(CuBr_2^-)_S$ complexes pass from the metallic surface to the bulk solution $(CuBr_2^-)_E$, this step being the controlling step:

$$(CuBr_2^-)_S \rightarrow (CuBr_2^-)_E \tag{3}$$

In summary, the corrosion of copper under flowing conditions in deaireated and concentrated LiBr solutions was controlled mainly by the mass transport of the $CuBr_2^-$ complexes from the metallic surface to the bulk solution through the CuBr film and the diffusion boundary layer [35].

Regarding the LiBr concentration effect, the corrosion potential values shift towards more active values as the concentration is higher. Figure 7 shows the corrosion potential evolution with the logarithm of the bromide concentration for every rotation rate value. Corrosion potential values vary linearly with the logarithm of the bromide concentration. This behaviour is the similar under static and dynamic conditions. Therefore, a higher bromide concentration favours copper corrosion.

3.4. Corrosion current density

Table 3 presents the corrosion current density for the different LiBr concentrations at the different rotation rates.

Table 3. Corrosion current density values (i_{corr}) of copper at the different rotation rates in the 400 g/l, 700 g/l, and 850 g/l LiBr solutions at 25 º C.

	i_{corr} ($\mu A/cm^2$)		
f (r.p.m.)	400 g/l LiBr	700 g/l LiBr	850 g/l LiBr
0	6	11	23
500	15	22	33
1000	25	31	42
1500	30	37	45
2000	39	44	50
2500	48	56	55
3000	53	60	61

The corrosion current density increases with the rotation rate [37]. The effect of increasing velocity is an increase of the surface concentration of the corrodent or a decrease of the surface concentration of the corrosion product. Therefore, the corrosion rate increases with increasing velocity. At 2500 r.p.m., and 3000 r.p.m. the corrosion current density increases with the LiBr concentration up to the 700 g/L, from this value the corrosion current density remains constant. At higher anion concentrations, the bromide anion can be absorbed on the electrode surface and showing down the corrosion process [38], corrosion that is favoured by the mobility of the anions at highest rotation rates. This can explain the stabilisation of the corrosion current density with the concentration at high rotation rates.

Corrosion current density values increase with the rotation rate at all the studied LiBr concentrations. If the diffusion of copper under flow conditions is governed by mass transport, a certain effect of fluid velocity on corrosion will be expected as a result of changes in the hydrodynamic

conditions. A general dependence of the corrosion rate on fluid velocity can be determined using the following potential relation between corrosion rate and Reynolds number [39-42]:

$$i_{corr} = \text{constant} \cdot Re^a \qquad (4)$$

Figure 8 a) shows the logarithm of i_{corr} versus the logarithm of the Reynolds number for the different LiBr concentrations used in the tests. The experimental exponent (a) in the equation 4 can be in the range from 1 to 3 depending upon the corrosion mechanism and flow regime. For mass transport the value of the exponent is closed to 1, while for erosion corrosion the value is up to 3. For mixed control of a chemical step and mass transport, the exponent value is between 1 and 0, depending on the mass transport. The exponent values obtained for the studied LiBr concentrations were: 0.70 for the 400 g/l LiBr solution, 0.56 for the 700 g/l LiBr solution, and 0.35 for the 850 g/l LiBr solution. According to the exponent, the control of the process is a mixed control between mass transport and chemical step. This exponent is lower as the LiBr concentration is higher. A greater number of bromide ions results in a higher diffusion rate. Therefore, at higher LiBr concentrations the control by diffusion decreases.

Figure 8 b) shows the Levich representation of the logarithm of i_{corr} versus the logarithm of the angular velocity □. The control of the process can also be studied through the Levich equation [43]. This equation relates the corrosion current density with the square root of the angular velocity. If the slope value $\Delta(\log i_{corr})/ \Delta(\log \omega \text{ (rad/s)})$ is 0.5, the process is under diffusion control [43]. The slope values for the different concentrations were: 0.30 for the 400 g/l LiBr solution, 0.24 for the 700 g/l LiBr solution, and 0.15 for the 850 g/l LiBr solution. All the slope values were lower than 0.5, i.e. the process was not under diffusion control.
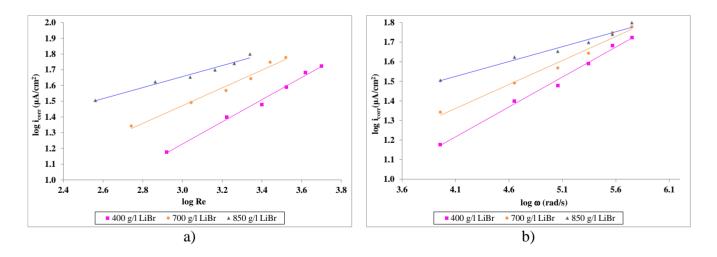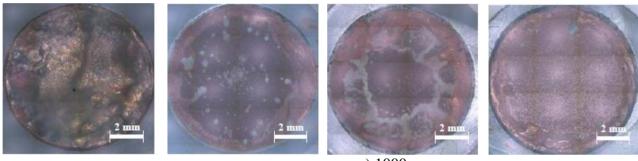

a)   b)

Figure 8. a) Logarithm of i_{corr} versus the logarithm of the Reynolds number in the different aqueous LiBr solutions at 25 ºC. b) Logarithm of i_{corr} versus the logarithm of the angular velocity □ in the different aqueous LiBr solutions at 25 ºC.

This confirms that the reaction is under mixed control and the influence of diffusion is lower as a consequence of the high LiBr concentration. This fact is in agreement with the corrosion potential, which indicated that the cathodic reaction was under activation control and the anodic reaction was under diffusion control. Then, the global reaction is under mixed control.

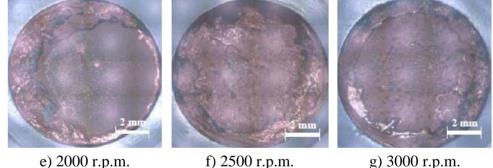### 3.5. Microscopic characterisation

Figures 9 to 11 show the images of the electrode surface after the test in the 400, 700 and 850 g/l LiBr solutions, respectively.

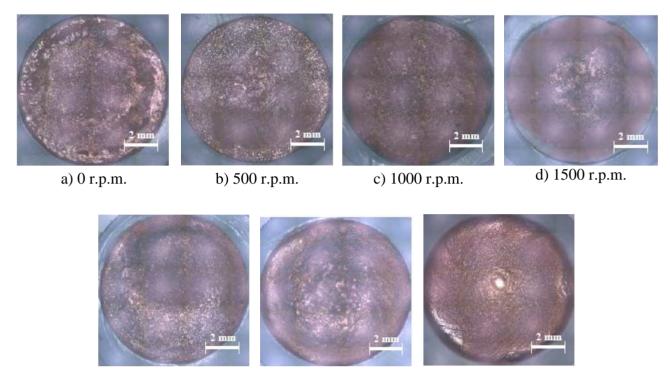a) 0 r.p.m.   b) 500 r.p.m.   c) 1000 r.p.m.   d) 1500 r.p.m.

e) 2000 r.p.m.   f) 2500 r.p.m.   g) 3000 r.p.m.

Figure 9. Images of the electrode surface after the tests in the 400 g/l LiBr solution at 25 ºC at the different rotation rates.

In the case of the 400 g/l LiBr solution, the surface is homogeneously attacked during the potentiodynamic curve under static conditions (Figure 9 a)). Under the dynamic conditions the peripheral area of the electrode is more severely affected than the central area. The extension of the peripheral area affected by corrosion is greater with the rotation rate (Figures 9 b) to 9 g)). Furthermore, the depth of the damage increases with the rotation rate and it is greater in the external area of the electrode surface. On the other hand, the final corrosion products that cover the electrode surface under the static conditions have different appearance than the corrosion products observed under dynamic conditions. This may be due to the removal of the layer of corrosion products by erosion, leading to the formation of new corrosion products. Furthemore, in the 400 g/l LiBr solutions
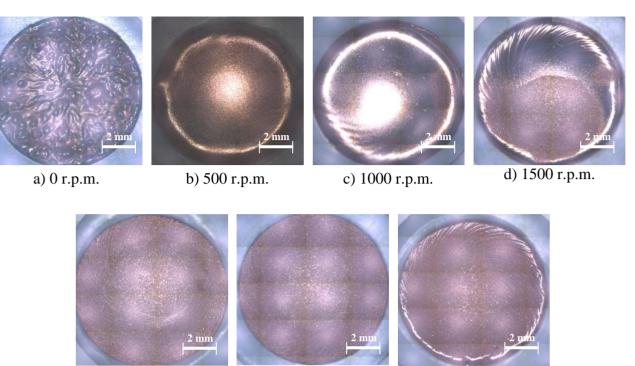
no flow lines appear at any rotation rate and the damage is greater in the external area of the electrode than in the centre.

a) 0 r.p.m.   b) 500 r.p.m.   c) 1000 r.p.m.   d) 1500 r.p.m.

e) 2000 r.p.m.   f) 2500 r.p.m.   g) 3000 r.p.m.

Figure 10. Images of the electrode surface after the tests in the 700 g/l LiBr solution at 25 ºC at the different rotation rates.

The images of the electrode surface after the polarisation curves in the 700 g/l LiBr solution show the effects of the hydrodynamic conditions (Figure 10). Under static conditions, generalised corrosion is observed without preferencial attacked areas (Figure 10 a)). Under dynamic conditions (Figures 10 b) to 10 g)), the damage on the electrode grows as the rotation rate increase and it is located at the peripheral area of the electrode surface. On the other hand, some flow lines appear in the tests at 2500 and 3000 r.p.m. These lines begin in the center of the sample in the case of the 3000 r.p.m. test and flow line are closer together than in the 2500 r.p.m test.

Tests carried out in the 850 g/l LiBr solution under static conditions show that the surface is homogenously attacked, the depth of the attack being higher than in the 400 and 700 g/l solutions (Figure 11 a)). On the other hand, at 500 r.p.m. the attack is deeper on the peripheral area than in the center of the electrode surface. At 1000 r.p.m, some flow lines appear in the electrode surface as the the rotation rate increases. The distance between the flow lines decreases and the center of the electrode surface is more severely affected. The depth of the attack also grows with the rotation rate and more material is lost. In the case of the test at 3000 r.p.m. the flow lines go from the center to the limit of the electrode surface, i.e. corrosion damage increases with the rotation rate and the number of flow lines is greater.

a) 0 r.p.m.   b) 500 r.p.m.   c) 1000 r.p.m.   d) 1500 r.p.m.

e) 2000 r.p.m.   f) 2500 r.p.m.   g) 3000 r.p.m.

Figure 11. Images of the electrode surface after the tests in the 850 g/l LiBr solution at 25 ºC at the different rotation rates.

4. CONCLUSIONS

Lithium bromide-water absorption machines powered by renewable energies can contribute to the rational utilisation of energy and the protection of the environment. In this work the effect of the hydrodynamic conditions and LiBr concentration on the corrosion of copper in LiBr solutions was studied. The main conclusions of this work are:

1. OCP and corrosion potential values decrease with the rotation rate and LiBr concentration.

2. The corrosion current density values increase with the rotation rate and LiBr concentration.

3. The cathodic reaction is under activation control and the anodic reaction is under diffusion control of corrosion products from the electrode surface.

4. The global process is under mixed control and the influence of diffusion decreases as the LiBr concentration increases.

5. The damage of the electrode surface is greater at high rotation rates increase and concentrations.

References

1. Council Decision of 14 October 1988 concerning the conclusion of the Vienna Convention for the protection of the ozone layer and the Montreal Protocol on substances that deplete the ozone layer, Official Journal L 297, 31/10/1988 p. 8-28. (2010).
2. http://unfccc.int, website of United Nations Framework Convention on Climate Change. (2010)
3. K. Tanno, M. Itoh, T. Takahashi, H. Yashiro, N. Kumagai. *Corros. Sci*. 34 (1993) 1441-1451
4. J J.W. Furlong. The Air Pollution Consultant (11/12 1994) 1.12.
5. M.T.Montañés R.Sanchez-Tovar, J. García-Antón, V. Pérez-Herranz. *Int. J. Electrochem. Sci*. 5 (2010), 1934.
6. Ahmed Y. Musa, Abdul Amir H. Kadhum, Abu Bakar Mohamad, Abdul Razak Daud, Mohd Sobri Takriff, Siti Kartom Kamarudin, Norhamidi Muhamad. *Int. J. Electrochem. Sci*. 4 (2009) 707.
7. E.Sarmiento, J.G.Gonzalez-Rodriguez, J.Uruchurtu, O.Sarmiento, M.Menchaca: *Int. J. Electrochem. Sci.*, 4 (2009) 144.
8. D.M. García-García, E. Blasco-Tamarit, J. García-Antón. *Int. J. Electrochem. Sci*. 6 (2011) 1237.
9. R.M. Fernández-Domene, E. Blasco-Tamarit, D.M. García-García, J. García-Antón. *Int. J. Electrochem. Sci.* 6 (2011) 3292.
10. R. Leiva-Garcia, J. Garcia-Anton, M.J. Muñoz-Portero. *Corros. Sci*. 52 (2010) 950.
11. R. Leiva-García, J. García-Antón, M.J. Muñoz-Portero. *Corros. Sci*. 52 (2010) 2133.
12. E. Blasco-Tamarit, A. Igual-Muñoz, J. Garcia-Antón, D. García-García. *Corros. Sci*. 50 (2008) 1848.
13. B.R. Tian, Y. F. Cheng. *Corros. Sci*. 50 (2008) 773.
14. G.A. Zhang, Y. F. Cheng. *Corros. Sci*. 51 (2009) 901.
15. Helmuth Sarmiento Klapper, Dionisio Valverde Custodio Vasquez. *Corros. Sci*. 50 (2008) 2718.
16. L. Robbiola, T.T.M. Tran, P. Dubot, O. Majerus, K. Rahmouni. *Corros Sci*. 50 (2008) 2205.
17. L. Cáceres, T. Vargas, L. Herrera. *Corros. Sci*. 51 (2009) 971.
18. M. Scendo, M. Hepel. *Journal of Electroanalytical Chemistry* 613 (2008) 35.
19. G. Kear, B.D. Barker, K.R. Stokes, F.C.Walsh. *Electrochim. Acta* 52 (2007) 2343.
20. Mohammed A.Amin. *Chinese Chemical Letters* 21 (2010) 341.
21. Mohammed A.Amin, K.F.Khaled: *Corros. Sci*. 52 (2010) 1194.
22. ASTM G-5 - 94. American Society for Testing and Materials. (1994).
23. J. Garcia Anton, A. Igual Muñoz, J.L. Guiñón, V. Pérez Herranz. Electro-Optical Method by On-line Visualization of Electrochemical Process and Experimental Process, Spain, P200002525 (2000).
24. J. García Antón, A. Igual Muñoz, J.L. Guiñón, V. Pérez Herranz. Horizontal Electrochemical Cell by the Electro-Optical Analysis of Electrochemical Process, Spain, P200002526 (2000).
25. J. García Antón, A. Igual Muñoz, J.L. Guiñón, V. Pérez Herranz, J. Pertusa-Grau. *Corrosion* 59 (2003) 172.
26. J. García Antón, A. Igual Muñoz, J.L. Guiñón, V. Pérez Herranz. *J. Appl. Electrochem*. 31 (2001) 1195.
27. Juin Chi Chen, Shiou-Ru Lin Went-TA Tsai. *Appl. Surf. Sci*. 233 (2004) 80.
28. N. Perez, Electrochemistry and Corrosion Science, Kluwer Academic Pub. MA, USA, (2004) 146.
29. D.H. Shen, W. Li, K. Nobe, *Interfinish* 92 (1992) 651.
30. I.C. Lavos-Valereto, I. Costa S. Wolynec. *Journal of Biomedical Materials Research. Applied Biomaterials* 63 (2002) 664.
31. S.L. de Assis, S. Wolynec, I. Costa. *Electrochim. Acta* 51 (2006) 1815.
32. G. P. Power, I. M Ritchie. *Electrochim. Acta* 23 (1981) 1073.
33. R.L. Brossard. *Can. J. Chem* 62 (1984) 36.
34. S. Magaino. *Electrochim. Acta* 42 (1997) 377.
35. V. Pérez-Herranz, M. T. Montañés, J. García-Antón, J. L. Guiñón. *Corrosion* 57 (2001) 835.

36. P.A. Lush, M. J. Carr. *Corros. Sci*. 19 (1979) 1079.
37. E. Sidot N. Souissi, L. Bousselmi, E. Triki, L. Robbiola. *Corros. Sci*. 48 (2006) 2241.
38. R. F. Tobias, Ken Nobe. *J. Electrochem. Soc*. 122 (1975) 65.
39. E. Heitz. *Electrochim. Acta* 41 (1996) 503.
40. E. Heitz. *Corrosion* 47 (1991) 135.
41. M.M. Stack, F. H. Stott, G. C. Wood. *Journal de Physique* IV 3 (1993) 687.
42. J.R. Shadley, S.A. Shirazi, E. Dayalan, E. F. Rybicki. *Corrosion* 54 (1998) 972.
43. V.G. Levich. Physicochemical Hydrodynamics (1962) Prentice-Hall